HIV-1 evolutionary dynamics under non-suppressive antiretroviral therapy

Steven A. Kemp[1,3*†], Oscar Charles[1†], Anne Derache[2], Collins Iwuji[2,5], John Adamson[2], Katya Govender[2], Tulio de Oliveira[2,6], Nonhlanhla Okesola[2], Francois Dabis[7,8], Darren P. Martin[9], on behalf of the French National Agency for AIDS and Viral Hepatitis Research (ANRS) 12249 Treatment as Prevention (TasP) Study Group, Deenan Pillay[1], Richard A. Goldstein[1] & Ravindra K. Gupta[2,3]

[1.] Division of Infection & Immunity, University College London, London, UK

[2.] Africa Health Research Institute, Durban, South Africa

[3.] Cambridge Institute of Therapeutic Immunology & Infectious Disease (CITIID), Cambridge, UK

[4.] Department of Medicine, University of Cambridge, Cambridge, UK

[5.] Research Department of Infection and Population Health, University College London, United Kingdom.

[6.] KRISP - KwaZulu-Natal Research and Innovation Sequencing Platform, UKZN, Durban, South Africa.

[7.] INSERM U1219-Centre Inserm Bordeaux Population Health, Université de Bordeaux, France.

[8.] Université de Bordeaux, ISPED, Centre INSERM U1219-Bordeaux Population Health, France.

[9.] Department of Integrative Biomedical Sciences, University of Cape Town, South Africa

[†]Authors contributed equally

Address for correspondence:
Steven A Kemp
Cambridge Institute for Therapeutic Immunology and Infectious Diseases
Jeffrey Cheah Biomedical Centre
Cambridge CB2 0AW, UK
sk2137@cam.ac.uk

or

Ravindra K Gupta
Cambridge Institute for Therapeutic Immunology and Infectious Diseases
Jeffrey Cheah Biomedical Centre
Cambridge CB2 0AW, UK
Rkg20@cam.ac.uk

Abstract

Prolonged virologic failure on 2nd-line protease inhibitor (PI) based ART without emergence of major protease mutations is well recognised and provides an opportunity to study within-host evolution in long-term viraemic individuals. Using next-generation sequencing and *in silico* haplotype reconstruction we analysed whole genome sequences from longitudinal plasma samples of eight chronically infected HIV-1 individuals failing 2nd-line regimens from the ANRS 12249 TasP trial. On non-suppressive ART, there were large fluctuations in synonymous and non-synonymous variant frequencies despite stable viraemia. Reconstructed haplotypes provided evidence for selective sweeps during periods of partial adherence, and viral haplotype competition during periods of low drug exposure. Drug resistance mutations in reverse transcriptase (RT) from earlier and current ART were used as markers of viral haplotypes in the reservoir and their distribution over time indicated recombination. We independently observed linkage disequilibrium decay, indicative of recombination. These data highlight dramatic changes in virus population structure that occur during stable viremia under non suppressive ART.

Introduction

Even though HIV-1 infections are most commonly initiated with a single founder virus [1], acute and chronic disease are characterised by extensive inter- and intra-participant genetic diversity [2,3]. The rate and degree of diversification is influenced by multiple factors, including selection pressures imposed by the adaptive immune system, exposure of the virus to drugs, and tropism/fitness constraints relating to replication and cell-to-cell transmission in different tissue compartments [4,5]. During HIV-1 infection, high rates of reverse transcriptase- (RT) related mutation and high viral turnover during replication result in swarms of genetically diverse variants[6] which co-exist as quasispecies. The existing literature on HIV-1 intrahost population dynamics is largely limited to untreated infections, predominantly in subtype B infected individuals[7-10]. These works have shown non-linear diversification of virus both towards and away from the founder strain during chronic untreated infection.

Viral population dynamics in long-term viraemic antiretroviral therapy (ART) treated individuals have not been characterised. HIV-1 rapidly accumulates drug-resistance associated mutations (DRMs), particularly during non-suppressive 1st-line ART[5,11]. As a result, ART-experienced participants failing 1st-line regimens for prolonged periods of time are characterised by high frequencies of common nucleoside reverse transcriptase (NRTI) and non-nucleoside reverse transcriptase (NNRTI) drug resistance mutations (DRMs) such as M184V, K65R and K103N [12]. Routinely, 2nd-line ART regimens consist of two NRTIs in conjunction with a boosted protease inhibitor (PI). Although PI DRMs are uncommonly reported [13], a situation that differs for less potent drugs used in the early PI era [5], multiple studies have indicated that diverse mutations accumulating in the *gag* gene during PI failure might impact PI susceptibility [14-20]. Common pathways for these diverse mutations have, however, been difficult to discern, likely reflecting multiple routes to drug escape.

Prolonged virological failure on PI-based regimens without the emergence of PI DRMs provides an opportunity to study evolution under partially-suppressive ART. The process of selective sweeps in the context of HIV-1 infection has previously been described [21,22] . Although major PI DRMs and other non-synonymous mutations in regulatory regions such as *pol,* can significantly lower fitness [2,23,24], these studies have been typically shown outside of the context of longitudinal sampling. HIV-1 has been shown to exhibit significant genetic diversity within infected hosts, with different populations of virus accumulating beneficial mutations – referred to as 'quasispecies' [25,26].

We have deployed next-generation sequencing of stored blood plasma specimens from participants in the Treatment as Prevention (TasP) ANRS 12249 study [27], conducted in Kwazulu-Natal, South Africa. All participants were infected with HIV-1 subtype C and characterised as failing 2nd-line regimens containing Lopinavir and Ritonavir (LPV/r), with prolonged virological failure in the absence of major known PI mutations[28]. In this manuscript, we report details of evolutionary dynamics during non-suppressive 2nd-line ART. By sampling participants consistently over several years, we propose that ongoing evolution is driven by the dynamic flux between genetic drift, fitness driven selection and recombination, exemplified by resistance mutations that have undergone reassortment across haplotypes through recombination.

Results

Participant Characteristics

Eight south African participants with virological failure of 2nd-line PI based ART and at least two timepoints, with viraemia above 1000 copies/ml were selected from the French ANRS TasP trial for viral dynamic analysis. Participant metadata collected included viral loads, regimens and time since ART initiation (**Table 1**). HIV RNA was isolated from venous blood samples and subject to whole-genome sequencing (WGS) using Illumina technology; from this whole-genome haplotypes were reconstructed. Prior to participation in the TasP trial, participants accessed 1st-line regimens for an average of 5.6yrs (±2.7yrs). At baseline enrolment into TasP (whilst failing 1st-line regimens), the median participant viral load was $4.96x10^{10}$ (IQR: $4.17x10^{10}$ – $5.15x10^{10}$); twelve DRMs were found at a threshold of >2%; the most common of which were the RT mutations. K103N, M184V and P225H, which are consistent with previous use of d4T, NVP, EFV and FTC/3TC. Six of the eight participants had minority frequency DRMs associated with PI failure (average 6.4%) which were usually seen only at single timepoints throughout the longitudinal sampling. Observed mutations included L23I, I47V, M46I/L, G73S, V82A, N83D and I85V (**Supplementary Tables 1a-3c**). Viral populations of four of the eight participants also carried major integrase stand inhibitor (INSTI) mutations, also at minority frequencies (average 5.0%) and also usually at single timepoints (T97A, E138K, Y143H, Q148K). Of note, participants were maintained on protease inhibitors during viremia as poor adherence was suspected as the reason for ongoing failure. Sanger sequencing where undertaken for clinical monitoring, had not detected major protease mutations, consistent with the NGS data (**Supplementary Tables 1a-3c**).

SNP frequencies and measures of diversity/divergence over time

WGS data was used to measure the changing frequencies of viral single nucleotide polymorphisms (SNPs) relative to a dual-tropic subtype C reference sequence (AF411967) within individuals over time (**Figure 1a-b**). The number of longitudinal synonymous SNPs mirrored the number of non-synonymous SNPs, but the former were two-to-three-fold more common. Diversification, determined by counting the number of SNPs relative to the refence sequence, was considered. There were dynamic changes in the numbers of SNPs over time, with both increases and decreases in numbers of SNPs, suggesting population competition, and/or the occurrence of selective sweeps. From timepoint two onwards (all participants now on 2nd-line, PI-containing regimens for >6 months), all participants (except 28545) had increases in both synonymous and non-synonymous SNPs.

In previous literature, viral populations within untreated, chronically infected HIV-1 patients have found to carry some reversion mutations to founder or infecting virus states[7]. We repeated this analysis with our chronically infected, but treated, HIV-1 population, considering separately the earliest consensus sequence, HIV-1 subtype C consensus and M group consensus sequences as founders strains. Divergence from the founder strain per, patient timepoint was measured by calculating the genetic distance between patient and founder for each longitudinal sample.

To assess if there was 1) a general trend of reversion to founder and 2) If time was an explanatory variable to that trend we utilised a Linear Mixed Effects Model (LMEM). Divergence from the founder was modelled as the response, each participant was treated as a random effect, and time from first patient sample treated as a fixed effect "time". Modelling the whole genome sequences indicated that there was no significant effect of time (in months) on viral diversification or reversion to consensus or ancestral C and M states (**Figures 1c-e, Supplementary table 2**).

When assessing the constituent 1000 bp genomic regions of each alignment, eight total genomic regions were significant for divergence (four from the ancestral C and four from the ancestral M) indicating time (in months) impacted viral divergence. This revealed that in portions of the genome (*pol*, *vpu* and *env*) there was sufficient statistical support to confirm that there was ongoing divergence from both the subtype C consensus and the subtype M consensus. However, correction for false discovery rate (FDR) with a Benjamini Hochberg correction revealed that divergence was only significant ($p<0.05$) for three 1000bp portions of the genome, respective to the subtype M consensus (**Supplementary Figure 1, Supplementary Table 2**). Divergence from these ancestral sequences is likely enabled by recombination, which unlinks hyper-variable loci from strongly

153 constrained neighbouring sites. We found no evidence for reversions and were therefore unable to
154 conclude that these patients are reverting to founder as described by Zanini et al (2015).
155
156 To assess the relationship of the observed divergence patterns, we examined nucleotide diversity by
157 considering all pairwise nucleotide distances of each consensus sequence, by timepoint and
158 participant using a multidimensional scaling approach[30]. Intra-participant nucleotide diversity varied
159 considerably between participants (**Figure 2a**). Viruses from some participants showed little diversity
160 between timepoints (e.g. participant 16207), whereas those from others showed higher diversity
161 between timepoints (e.g. participant 22763). In some instances a participant's viruses were tightly
162 clustered, suggesting little change over time (**Figure 3a,** participants 16207, 26892 & 47939),
163 compared to others (participants 22828 & 28545). To corroborate the MDS approach, we used an
164 alternative novel method of examining nucleotide diversity of longitudinal timepoints using all
165 positional information from BAM files (**Supplementary Figure 2**).
166
167 **Phylogenetic analysis of inferred haplotypes**
168 The preceding diversity assessments suggested the existence of distinct viral haplotypes within each
169 participant. We therefore used a recently reported computational tool[29] to infer 289 unique
170 haplotypes across all participants, with between 11 and 32 haplotypes (average 21) per participant.
171 The number haplotypes changed dynamically between successive timepoints indicative of
172 dynamically shifting populations (**Figure 2B**). To confirm plausibility of haplotypes, a phylogeny of all
173 consensus sequences was inferred (**Supplementary Figure 3**) and a MDS plot of all viral haplotypes
174 was constructed (**Supplementary Figure 4**).
175
176 **Linkage Disequilibrium and Recombination**
177 LD between two pairwise loci is reduced by recombination, such that LD tends to be higher for loci
178 that are close and lower for more distant loci[31]. HIV-1 is known to recombine such that sequences
179 are not generally in linkage disequilibrium (LD) beyond 400bp[7]. The significance of recombination in
180 an intra-host, single infection setting is less well understood[32]. To assess whether intra-patient
181 recombination was occurring between the haplotypes observed in each of the three most sampled
182 participants, we determined LD decay patterns. We assumed that if there was random
183 recombination, this would equate to smooth LD decay patterns. This was not observed. Rather,
184 each participant demonstrated a complex decay pattern, consistent with non-random
185 recombination along the genome (**Figure 3A).** Given this, we characterised recombination patterns
186 (**Figure 3b**). Inferred recombination breakpoints were identified within participants over successive

timepoints (**Supplementary Figure 5**). DRMs were accumulated over successive timepoints for participant 22763, whereas in participant 15664 the reverse was true. Participant 16207 had recombinant breakpoints localised in the *pol* gene in two timepoints, though it retained its majority DRM (K103N) across all haplotype populations, possibly as a result of K103N being acquired as a transmitted DRM.

Changing landscapes of non-synonymous and synonymous mutations

In the absence of major PI mutations, we first examined non-synonymous mutations across the whole genome (**Figures 4-6**), with a specific focus on *pol* (to identify known first and second line NRTI-associated mutations) and *gag* (given its known involvement in PI susceptibility). We and others have previously shown that *gag* mutations accumulate during non-suppressive PI therapy[33,34]. There are also data suggesting associations between *env* mutations and PI exposure [35,36]. **Supplementary Tables 1-3** summarise the changes in variant frequencies of *gag*, *pol* and *env* mutations in participants over time. We found between two and four mutations at sites previously associated with PI resistance in each participant, all at persistently high frequencies (>90%) even in the absence of presumed drug pressure. This is explained by the fact that a significant proportion of sites associated with PI exposure are also polymorphic across HIV-1 subtypes[18,37]. To complement this analysis, we examined underlying synonymous mutations across the genome. This revealed complex changes in the frequencies of multiple nucleotide residues across all genes. These changes often formed distinct 'chevron-like' pattens between timepoints (**Figures 4c & 5b**), indicative of linked alleles dynamically shifting, which is in turn suggestive of competition between viral haplotypes.

Participant 15664 had consistently low plasma concentrations of all drugs at each measured timepoint, with detectable levels measured only at month 15 and beyond (**Figure 4a**). At baseline, whilst on NNRTI-based 1st-line ART, known NRTI (M184V) and NNRTI (K103N and P225H) DRMs[5] were at high prevalence in the virus populations; which is as expected whilst adhering to 1st-line treatments. Haplotype reconstruction and subsequent analysis inferred the presence of a majority haplotype carrying all three of these mutations at baseline, as well as a minority haplotype with the absence of P225H (**Figure 4d**, dark grey circles). Following the switch to a 2nd-line regimen, variant frequencies of M184V and P225H dropped below detection limits (<2% of reads), whilst K103N remained at high frequency (**Figure 4B**). Haplotype analysis was concordant, revealing that viruses with K103N, M184V and P225H were replaced by haplotypes with only K103N (**Figure 4D**, light grey circles). At timepoint two (month 8), there were also numerous synonymous mutations observed at

high frequency in both *gag* and *pol* genes, corresponding with the switch to a 2nd-line regimen. At timepoint three (15 months post-switch to 2nd-line regimen) drug concentrations were highest, though still low in absolute terms, indicating partial adherence. Between timepoints three and four we observed a two-log reduction in viral load, with a modest change in frequency of RT DRMs. However, we observed synonymous variant frequency shifts predominantly in both *gag* and *pol* genes, as indicated by multiple variants increasing and decreasing contemporaneously, creating characteristic chevron patterning (**Figure 4b**). However many of the changes were between intermediate frequencies, (e.g. between 20% and 60%), which differed from changes between time points one and two where multiple variants changed more dramatically in frequency from <5% to more than 80%, indicating harder selective sweeps. These data are in keeping with a soft selective sweep between time points three and five. Between timepoints five and six, the final two samples, there was another population shift - M184V and P225H frequencies fell below the detection limit at timepoint six, whereas the frequency of K103N dropped from almost 100% to around 80% (**Figure 4b**). This was consistent with the haplotype reconstruction, which inferred a dominant viral haplotype at timepoint six bearing only K103N, as well as three minor haplotype with no DRMs at all (**Figure 4d**, light blue circles).

The phylogeny of inferred haplotype sequences showed that haplotypes from all timepoints were interspersed throughout the tree (except at timepoint 4, which remained phylogenetically distinct). This is indicative of ongoing viral population competition. DRMs showed some segregation by clade; viruses carrying a higher frequency of DRMs (M184V, P225H and K238T) were observed in clade A (**Figure 4d**), and those with either K103N alone, or no DRMs were preferentially located clade C (**Figure 4d**). However, this relationship was not clear cut, and therefore consistent with competition between haplotypes during low drug exposure. Soft sweeps were evident, given the increasing diversity (**Figure 1, Supplementary Figure 4**) of this participant.

Participant 16207. Viral load in this participant were consistently above 10,000 copies/ml (**Figure 5a)**. As with participant 15664, detectable drug concentrations in blood plasma were either extremely low or absent at each measured timepoint, consistent with non-adherence to the prescribed regimen. There was little change in the frequency of DRMs throughout the follow-up period, even when making the switch to the 2nd-line regimen. NNRTI resistance mutations such as K103N are known to have minimal fitness costs[24] and can therefore persist in the absence of NNRTI pressure. Throughout treatment the viruses from this participant maintained K103N at a frequency of >85% but also carried an integrase strand transfer inhibitor (INSTI) associated mutation (E157Q)

and PI-exposure associated amino acid replacements (L23I and M46I) at low frequencies at timepoints two and three. Despite little change in DRM site frequencies, very significant viral population shifts were observed at the whole genome level; again indicative of selective sweeps (**Figures 5b-c**). Between timepoints one and four, several linked mutations changed abundance contemporaneously, generating chevron-like patterns of non-synonymous changes in *env* specifically (blue lines, **Figure 5b**). A large number of alleles increased in frequency from <40% to >80% at timepoint one, followed by decreases in frequency from >70% to <30% at timepoint three. Whereas large shifts in *gag* and *pol* alleles also occurred, the mutations involved were almost exclusively synonymous (red and green lines).

Phylogenetic analysis of inferred whole genome haplotypes again showed a distinct cladal structure as observed in participant 15664 (**Figure 5d**), although the dominant haplotypes were equally observed in the upper clade (A) and lower clade (C) (**Figure 5d**). K103N was the majority DRM at all timepoints, except for a minority haplotype at timepoint three, also carrying E157Q. Haplotypes did not cluster by time point. Significant diversity in haplotypes from this participant was confirmed by MDS (**Supplementary Figure 4**).

Participant 22763 was notable for a number of large shifts in variant frequencies across multiple drug resistance associated residues and synonymous sites. Drug plasma concentration for different drugs was variable yet detectable at most measured timepoints reflecting changing levels of adherence across the treatment period (**Figure 6a).** Non-PI DRMs such as M184V, P225H and K103N were present at baseline (time of switch from first to second line treatments). These mutations persisted despite synonymous changes between time points one and two. Most of the highly variable synonymous changes in this participant were found in the *gag* and *pol* genes (as in participant 16207) (**Figure 6c**), but in this case *env* displayed large fluctuations in synonymous and non-synonymous allelic frequencies over time. At timepoint three, therapeutic concentrations of boosted lopinavir (LPV/r) and tenofovir (TDF) were measured in plasma and haplotypes clustered separately from the first two timepoints (**Figure 6d**, light and dark grey circles). NGS confirmed that the D67N, K219Q, K65R, L70R, M184V DRMs and NNRTI-resistance mutations were present at low frequencies from timepoint three onwards. Of note, between timepoints three and six, therapeutic concentrations of TDF were detectable, and coincided with increased frequencies of the canonical TDF DRM, K65R[5]. The viruses carrying K65R outcompeted those carrying the thymidine analogue mutants (TAMs) D67N and K70R, whilst the lamivudine (3TC) associated resistance mutation, M184V, persisted throughout. In the final three timepoints M46I emerged in *protease*, but never

289 increased in frequency above 6%. At timepoint seven, populations shifted again with some
290 haplotypes resembling those previously seen in timepoint four, with D67N and K70R again being
291 predominant over K65R in *reverse transcriptase* (**Figure 6d**, green and blue circles). At the final
292 timepoint (eight) the frequency of K103N was approximately 85% and the TAM-bearing populations
293 continued to dominate over the K65R population, which at this timepoint had a low frequency.
294
295 Although the DRM profile suggested the possibility of a selective sweep, we observed the same
296 groups of other non-synonymous or synonymous alleles exhibiting dramatic frequency shifts, but to
297 a lesser degree than in participants 16207 and 15664 i.e. 'chevron patterns' were less pronounced,
298 outside of the *env* gene (**Figure 6b-c**). Variable drug pressures placed on the viral populations
299 throughout the 2nd-line regimen appear to have played some role in limiting haplotype diversity.
300 Timepoints 1-4 all formed distinct clades, without intermingling, indicating that competition
301 between populations was not occurring to the same degree as in previous participants. Some
302 inferred haplotypes had K65R and others the TAMs D67N and K70R. K65R was not observed in
303 combination with D67N or K70R, consistent with previously reported antagonism between K65R and
304 TAMs whereby these mutations are not commonly found together within a single genome[38-40]. One
305 possible explanation for the disconnect between the trajectories of DRM frequencies over time and
306 haplotype phylogeny is competition between different viral populations. Alternatively, emergence of
307 haplotypes from previously unsampled reservoirs with different DRM profiles is possible, but one
308 might have expected other mutations to characterise such haplotypes that would manifest as
309 changes in the frequencies of large numbers of other mutations.
310
311 **Discussion**
312 The proportion of people living with HIV (PLWH) who are accessing ART has increased from 24% in
313 2010, to 68% in 2020[41,42]. However, with the scale-up of ART, there has also been an increase in both
314 pre-treatment drug resistance (PDR)[43,44] and acquired drug resistance[12,45] to 1st-line ART regimens
315 containing NNRTIs. Integrase inhibitors (specifically dolutegravir) are now recommended for first-
316 line regimens by the WHO in regions where PDR exceeds 10%[46]. Boosted PI-containing regimens
317 remain second line drugs following first 1st-line failure, though one unanswered question relates to
318 the nature of viral populations during failure on PI-based ART where major mutations in *protease*,
319 described largely for less potent PIs, have not emerged. Here we have comprehensively analysed
320 viral populations present in longitudinally collected plasma samples of chronically-infected HIV-1
321 participants under non-suppressive 2nd-line ART.
322

With the vast majority of PLWH ho have been treated in the post-ART era, virus dynamics during non-suppressive ART are important to understand, as there may be implications for future therapeutic success. For example, broadly neutralising antibodies (bNab) are being tested not only for prevention, but also as part of remission strategies in combination with latency reversal agents. We know that HIV sensitivity to broadly neutralising antibodies (bNab) is dependent on *env* diversity[47,48], and therefore prolonged ART failure with viral diversification could compromise sensitivity to these agents.

Our understanding of virus dynamics largely stems from studies that were limited to untreated individuals[10], with mostly subgenomic data analysed rather than whole genomes[10]. Traditional analyses of quasispecies distributions, for example as reported by Yu et al[49], suggest that viral diversity increases in longitudinal samples. However the findings of Yu et al were based entirely on short-read NGS data without considering whole-genome haplotypes. The added benefit of examining whole genomes is that linked mutations can be identified statistically using an approach that we recently developed[29]. Indeed, haplotype reconstruction has proved beneficial in the analysis of compartmentalisation and diversification of several RNA viruses, including HIV-1, CMV and SARS-CoV-2[33,50,51].

Key findings of this study were, firstly that diversity as defined by the number of quasispecies in each sample, typically increased over time. Considering divergence, (a measure at consensus level for how many mutations have accumulated in a current sequence, from the founder infection) in contrast to previous literature which showed that there was a degree of reversion to the founder strain[7], we show that there was no significant reversion in our study population. There was also no significant divergence from baseline, ancestral C or ancestral M consensus sequences when considering the whole genome. However, when considering 1000bp fragments of the genome in a sliding window, several regions in *pol*, *vpu* and *env* significantly diverged from the consensus C and consensus M sequences.

A second key finding in our study was that synonymous mutations were generally two-to-three fold more frequent than non-synonymous mutations during non-suppressive ART during chronic infection - a finding in contrast to that seen previously in a longitudinal study of untreated individuals[2]. Non-synonymous changes were enriched in known polymorphic regions such as *env* whereas synonymous changes were more often observed to fluctuate in the conserved *pol* gene. This finding may reflect early versus chronic infection and differing selective pressures. Haplotype

357 reconstruction revealed evidence for competing haplotypes, with phylogenetic evidence for
358 numerous soft selective sweeps in that haplotypes intermingled during periods where there were
359 low drug concentrations measured in the blood plasmas of participants .
360
361 Individuals in the present study were treated with Ritonavir boosted Lopinavir along with two NRTIs
362 (typically Tenofovir + Emtricitabine). We observed significant changes in the frequencies of NRTI
363 mutations in two of the three participants studied in-depth. These fluctuations likely reflected
364 adherence to the 2nd-line regimen though we saw evidence for possible archived virus populations
365 with DRMs emerging during follow-up in that large changes in DRM frequency were not always
366 accompanied by changes at other sites. This is consistent both with the occurrence of soft selective
367 sweeps and previous observations that non-DRMs do not necessarily drift with other mutations to
368 fixation[21]. As frequencies of RT DRMs did not always segregate with haplotype frequencies (i.e. the
369 same mutations were repeatedly observed on different genetic backgrounds), we suggest that a
370 high number of recombination events, known to be common in HIV infections, were likely
371 contributing to the observed haplotypic diversity.
372
373 Although no participant developed major resistance mutations to PIs at consistently high
374 frequencies (https://hivdb.stanford.edu/dr-summary/resistance-notes/PI/), we did observe non-
375 synonymous mutations in *gag* which have been previously associated to mediate resistance to PI.
376 There was, however, no temporal evidence of specific mutations being associated with selective
377 sweeps. For example, PI exposure-associated residues in matrix (positions 76 and 81) were observed
378 in participant 16207 prior to PI initiation[52]. Furthermore, participant 16207 was one of two
379 participants who achieved low-level viraemic suppression (45-999 copies/ml) of viral replication at
380 one or two timepoints. After both of these partial suppressions, the rebound populations appeared
381 to be less diverse, consistent with drug-resistant viruses re-emerging.
382
383 Mutations at sites in the HIV genome that are further apart than 100bp are subject to frequent
384 shuffling via recombination[53]. Unlike the smooth LD decay curves for pairs of HIV mutations reported
385 in the literature, we identified complex LD decay patterns within the genomes of viruses from
386 individual patients: patterns indicative of non-random recombination. Recombination appears as the
387 loss and gain of common genomic regions over successive timepoints between each participant's
388 haplotype populations (**Figure 3B**). Viruses from participant 15664 with inter-haplotype
389 recombination events detectable in the *vif* and *vpr* genes were present at four of the six analysed
390 timepoints. In contrast, viruses in participant 22763 had evidence of inter-haplotype recombination

events in the *gag-pol* genes were present at three of the eight analysed timepoints. We explain these recombination events detectable in longitudinally sampled sequences, as reflected in the previously discussed 'chevron' patterns whereby variants increase and subsequently decrease between timepoints. HIV quasispecies foster a degree of genetic diversity that facilitate rapid adaptive evolution through recombination whenever there exists within the quasispecies combinations of mutations that provide fitness advantages[26]. The relationship between recombination and the accumulation of multiple DRMs within individual genomes is not clearly evident within the analysed sequence datasets, with viruses sampled from each patient showing unique patterns of recombination. Inter-haplotype recombinants detected at timepoints two and six in participant 16207 had recombination events in *pol* that involved the transfer of the major DRM, K103N. Three independent Inter-haplotype recombination events detected in *pol* of participant 22763 viruses at timepoints two, four and six resulted in no change in DRMS at timepoint two, the gain of DRMS at timepoint four and loss of DRMs at timepoint six. The recombination dynamics in this patient were occurring against a backdrop of apparent antagonism between TAMs and DRMs (K65R and D67N). Finally, participant 15664 steadily lost DRMs throughout the longitudinal sampling period, although we found no evidence of recombination being implicated in this loss. This suggests that, in the absence of strong drug pressures, viral populations only maintained DRMs which were crucial for providing resistance to drugs that the participant was variably adhering to at the time.

Phylogenetic analyses of whole genome viral haplotypes demonstrated two common features: (1) evidence for selective sweeps following therapy switches or large changes in plasma drug concentrations, with hitchhiking of synonymous and non-synonymous mutations; and (2) competition between multiple viral haplotypes that intermingled phylogenetically alongside soft selective sweeps. The diversity of viral populations was maintained between successive timepoints with ongoing viremia, particularly in *env*. Changes in haplotype dominance were often distinct from the dynamics of drug resistance mutations in *reverse transcriptase* (RT), indicating the presence of softer selective sweeps and/or recombination.

This study had some limitations – we examined in-detail only three participants with ongoing viraemia and variable adherence to 2nd-line drug regimens. Despite the small sample size, this type of longitudinal sampling of ART-experienced participants is unprecedented. We are confident that the combination of computational analyses has provided a detailed understanding of viral dynamics under non-suppressive ART that will be applicable to wider datasets. The method used to reconstruct viral haplotypes *in silico* is novel and has previously been validated in HIV-1 positive

participants coinfected with CMV[50]. We are confident that the approach implemented by HaROLD has accurately, if conservatively, estimated haplotype frequencies and future studies should look to validate these frequencies using an *in vitro* method such as single genome amplification. Despite there being high viral loads present at each of the analysed timepoints, nuances of the sequencing method led in some cases to suboptimal degrees of gene coverage, particularly in the *env* gene. To ensure that uneven sequencing coverage did not bias our analyses, we ensured that variant analysis was only performed where coverage was >10 reads.

In summary we have found compelling evidence of HIV-1 within-host viral diversification, recombination and haplotype competition during non-suppressive ART. In future , participants failing PI-based regimens are likely to be switched to INSTI-based ART (specifically Dolutegravir in South Africa) prior to genotypic typing or resistance analysis. Although the prevalence of underlying major INSTI resistance mutations is low in sub-Saharan Africa[54,55], data linking individuals with NNRTI resistance with poorer virological outcomes on Dolutegravir[56], coupled with a history of intermittent adherence, warrant further investigation. Having shown that long-time intra-host PI failure increases the intra-patient diversity of HIV viral populations, monitoring future drug-failure cases will be of interest due to their capacity to maintain a reservoir of transmissible drug-resistant viruses, as well as impacting responses to future therapies.

Methods

Study & Participant selection

This cohort was nested within the French ANRS 12249 Treatment as Prevention (TasP) trial [27]. TasP was a cluster-randomised trial comparing an intervention arm who offered ART after HIV diagnosis irrespective of participant CD4 + count, to a control arm which offered ART according to prevailing South African guidelines. A subset of 44 longitudinal samples from eight chronically infected participants. Participants were selected for examination if there were >3 timepoint samples available. All samples were collected from blood plasma. The Illumina MiSeq platform was used and an adapted protocol for sequencing[57]. Adherence to 2nd-line regimens was measured by HPLC using plasma concentration of drug levels as a proxy. Drug levels were measured at each timepoint with detectable viral loads, post-PI initiation.

Ethical approval was originally grant by the Biomedical Research Ethics Committee (BFC 104/11) at the University of KwaZulu-Natal, and the Medicines Control Council of South Africa for the TasP trial

(Clinicaltrials.gov: NCT01509508; South African Trial Register: DOH-27-0512-3974). The study was also authorized by the KwaZulu-Natal Department of Health in South Africa. Written informed consent was obtained from all participants. Original ethical approval also included downstream sequencing of blood plasma samples and analysis of those sequences to better understand drug resistance. No additional ethical approval was required for this.

Illumina Sequencing

Sequencing of viral RNA was performed as previously described by Derache et al [58] using a modified protocol previously described by Gall et al [59]. Briefly, RNA was extracted from 1ml of plasma with detectable viral load of >1000 copies/ml, using QIAamp Viral RNA mini kits (Qiagen, Hilden, Germany), and eluted in 60µl of elution buffer. The near-full HIV genome was amplified with four HIV-1 subtype C primer pairs, generating 4 overlapping amplicons of between 2100 and 3900kb.

DNA concentrations of amplicons were quantified with the Qubit dsDNA HS Assay kit (Invitrogen, Carlsbad, CA). Diluted amplicons were pooled equimolarly and prepared for library using the Nextera XT DNA Library preparation and the Nextera XT DNA sample preparation index kits (Illumina, San Diego, CA), following the manufacturer's protocol.

Genomics & Bioinformatics

Poor quality reads (with Phred score <30) and adapter sequences were trimmed from FastQ files with TrimGalore! v0.6.519 [60] and mapped to a dual-tropic, clade C, south African reference genome (AF411967) with minimap2[61]. The reference genome was manually annotated in Geneious Prime v2020.3 with DRMs according to the Stanford HivDB [62]. Optical PCR duplicate reads were removed using Picard tools (http://broadinstitute.github.io/picard). Finally, QualiMap2 [63] was used to assess the mean mapping quality scores and coverage in relation to the reference genome for the purpose of excluding poorly mapped sequences from further analysis. Single nucleotides polymorphisms (SNPs) were called using VarScan2 [64] with a minimum average quality of 20, minimum variant frequency of 2% and in at least 10 reads. These were then annotated by gene, codon and amino acid alterations using an in-house script [65] modified to utilise HIV genomes.

All synonymous variants and DRMs were examined, and their frequency compared across successive timepoints. Synonymous variants were excluded from analysis if their prevalence remained at ≤10% or ≥90% across all timepoints. DRMs were retained for analysis if they were present at over 2%

492 frequency and on at least two reads. A threshold of 2% is supported by a study evaluating different
493 analysis pipelines, which reported fewer discordances over this cut-off [66].
494
495 **Measuring Divergence or Reversion to Baseline, Consensus C & Consensus M ancestors**
496 To assess patient divergence or reversion to founder we first needed consensus genomes, three
497 types of founder were used. The full length HIV-1 subtype C consensus was download from the LANL
498 HIV database and annotations from the subtype C reference sequence (AF411967.3) used for
499 haplotype reconstruction were transferred to this genome using Geneious Prime v2021.1.0 to
500 ensure positions remained consistent throughout. For the subtype M consensus, all full-length HIV-1
501 subtype A, B, C, D, F, G & H refence genomes were downloaded from the LANL HIV database and a
502 consensus of all of these was made using Geneious Prime v2021.1.0 with the 60% majority option.
503 Again, annotations were transferred from the AF411967.3 reference genome to ensure consistent
504 positioning.
505
506 For each patient divergence over time from inferred founder state was measured for 1) the baseline
507 sequence for each participant; 2) a reconstructed subtype C consensus; and 3) a reconstructed
508 subtype M consensus. Divergence was measures as the pairwise distance between timepoint
509 consensus and founder, calculated using the dist.dna() package with a TN93 nucleotide-nucleotide
510 substitution matrix and with pairwise deletion as implemented in the R package Ape v.5.4.
511
512 **Linear Mixed Effects Models**
513 To investigate the general relationship of time in months to divergence, incorporating all 8
514 participants, we built a series of Linear Mixed Effect Models implemented in the lmer R package.
515 Divergence was treated as the response, time as a fixed effect and participant as a random effect.
516 We built similar models for the whole genome & discrete genomic portions analysis, for each
517 founder strain. We tested if time had a non-0 effect on divergence by calculating p value using
518 Satterthwaite's method as imple,ented in the lmerTEst package. For the 1000bp analyses, a
519 Benjamini Hochberg correction adjustment was undertaken to account for 9 tests within the same
520 sample.
521
522 **Haplotype Reconstruction & Phylogenetics**
523 Whole-genome viral haplotypes were constructed for each participant timepoint using HaROLD
524 (Haplotype Reconstruction for Longitudinal Samples)[29]. The first stage consists of SNPs being
525 assigned to each haplotype such that the frequency of variants is equal to the sum of the

frequencies of haplotypes containing a specific variant. This considers the frequency of haplotypes in each sample, the base found at each position in each haplotype and the probability of erroneous measurements at that site. Maximal log likelihood was used to optimise time-dependent frequencies for longitudinal haplotypes which was calculated by summing over all possible assignment of haplotype variants. Haplotypes were then constructed based on posterior probabilities.

After constructing haplotypes, a 2nd stage or refinement process remaps reads from BAM files to constructed haplotypes. This begins with the *a posteriori* probability of each base occurring at each site in each haplotype from the first stage, but relaxes the assumption that haplotypes are identical at each sample timepoint and instead uses variant co-localisation to refine haplotype predictions. Starting with the estimated frequency of each haplotype in a sample, haplotypes are optimised by probabilistically assigning reads to the various haplotypes. Reads are then reassigned iteratively until haplotype frequencies converge. The number of haplotypes either increases or decreases as a result of combination or division according to AIC scores, in order to present the most accurate representation of viral populations at each timepoint.

Whole-genome nucleotide diversity was calculated from BAM files using an in-house script (https://github.com/ucl-pathgenomics/NucleotideDiversity). Briefly diversity is calculated by fitting all observed variant frequencies to either a beta distribution or four-dimensional Dirichlet distribution plus delta function (representing invariant sites). These parameters were optimised by maximum log likelihood.

Maximum-likelihood phylogenetic trees and ancestral reconstruction were performed using IQTree2 v2.1.3[67] and a GTR+F+I model with 1000 ultrafast bootstrap replicates[68]. All trees were visualised with Figtree v.1.4.4 (http://tree. bio.ed.ac.uk/software/figtree/), rooted on the AF411967.3 reference sequence, and nodes arranged in descending order. Phylogenies were manipulated and annotated using ggtrree v2.2.4.

Multi Dimension Scaling (MDS) Plots

Pairwise distances between these consensus sequences were calculated using the dist.dna() package, with a TN93 nucleotide-nucleotide substitution matrix and with pairwise deletion implemented in the R package Ape v.5.4. Non-metric Multi-dimensional scaling (MDS) was implemented using the metaMDS() function in the R package, vegan v2.5.7. MDS is a method to

attempt to simplify high dimensional data into a simpler representation of reducing dimensionality whilst retaining most of the variation relationships between points. We find that like network trees, non-metric MDS better represents the true relative distances between sequences, whereas eigenvector methods are less reliable in this sense. In a genomics context we can apply dimensionality reduction on pairwise distance matrices, where each dimension is a sequence with data points of n-1 sequences pairwise distance. The process was repeated with whole genome haplotype sequences.

Linkage Disequilibrium & Recombination

Starting with a sequence alignment we determined the pairwise LD r^2 associations for all variable sites using WeightedLD [69] without weighting. This method allowed us to exclude sites with any insertions or ambiguous characters easily where we used the option --min-acgt 0.99 and --min-variability 0.05. The pairwise R^2 values were then binned per 200bp comparison distance blocks along the genome and the mean R^2 value were taken and represented graphically to assess LD decay. This analysis was run for the three participants taken forward for in-depth analysis and run using an alignment of all their timepoint samples. Graphics were generated using Rv4.04.

We first performed an analysis for detecting individual recombination events in individual genome sequences using the RDP, GENECONV, BOOTSCAN, MAXCHI, CHIMAERA, SISCAN, and 3SEQ methods implemented in RDP5[70] with default settings. Putative breakpoint sites were identified and manually checked and adjusted if necessary using the BURT method with the MAXCHI matrix and LARD two breakpoint scan methods. Final recombination breakpoint sites were confirmed if at least three or more methods supported the existence of the recombination breakpoint.

Funding

SAK is supported by the Bill and Melinda Gates Foundation: OPP1175094. RKG is supported by Wellcome Trust Senior Fellowship in Clinical Science: WT108082AIA. OC is supported by a PhD studentship/UKRI MRC grant: MR/N013867/1. DPM is funded by The Wellcome Trust (222574/Z/21/Z).

Competing Interests

RKG has received ad hoc consulting fees from Gilead, ViiV and UMOVIS Lab.

Author Contributions

Conceptualization of study: S.A.K, R.K.G, A.D, Bioinformatic processes: A.D, S.A.K, O.C, D.P.M, Writing and revising manuscript: S.A.K, O.C, A.D, D.P.M, D.P, R.A.G, R.K.G.

Data Availability Statement

All bam files used to undertake analyses have been deposited on the SRA database with the following accession numbers SRR15510046 - SRR15510072.

Code Availability Statement

Custom code used to produce figures and graphs can be found at: https://github.com/Steven-Kemp/21-2_hiv_tasp/tree/main/scripts or within the references manuscripts.

Acknowledgements

The TasP trial was sponsored by the French National Agency for AIDS and Viral Hepatitis Research (ANRS; grant number, 2011-375), and funded by the ANRS, the Deutsche Gesellschaft für Internationale Zusammenarbeit (GIZ; grant number, 81151938), and the Bill & Melinda Gates Foundation through the 3ie Initiative. This trial was supported by Merck and Gilead Sciences, which provided the Atripla drug supply. The Africa Health Research Institute, (previously Africa Centre for Population Health, University of KwaZulu-Natal, South Africa) receives core funding from the Wellcome Trust, which provided the platform for the population-based and clinic-based research at the centre. We thank Alpha Diallo and Severine Gibowski at the ANRS for pharmacovigilance support, and Jean-François Delfraissy (director of ANRS). We thank the study volunteers for allowing us into their homes and participating in this trial, and the KwaZulu-Natal Provincial and the National Department of Health of South Africa for their support of this study. We thank staff of the Africa Health Research Institute for the trial implementation and analysis of data, including those who did the fieldwork, provided clinical care, developed and maintained the database, entered the data, and verified data quality.

References

1 Abrahams, M. R. *et al.* Quantitating the multiplicity of infection with human immunodeficiency virus type 1 subtype C reveals a non-poisson distribution of transmitted variants. *J Virol* **83**, 3556-3567, doi:10.1128/JVI.02132-08 (2009).

2 Zanini, F., Puller, V., Brodin, J., Albert, J. & Neher, R. A. In vivo mutation rates and the landscape of fitness costs of HIV-1. *Virus Evol* **3**, vex003, doi:10.1093/ve/vex003 (2017).

627 3 Salemi, M. The intra-host evolutionary and population dynamics of human
628 immunodeficiency virus type 1: a phylogenetic perspective. *Infect Dis Rep* **5**, e3,
629 doi:10.4081/idr.2013.s1.e3 (2013).
630 4 Lemey, P., Rambaut, A. & Pybus, O. G. HIV evolutionary dynamics within and among hosts.
631 *Aids Reviews* **8**, 125-140 (2006).
632 5 Collier, D. A., Monit, C. & Gupta, R. K. The Impact of HIV-1 Drug Escape on the Global
633 Treatment Landscape. *Cell host & microbe* **26**, 48-60, doi:10.1016/j.chom.2019.06.010 (2019).
634 6 Biebricher, C. K. & Eigen, M. What is a quasispecies? *Curr Top Microbiol Immunol* **299**, 1-31,
635 doi:10.1007/3-540-26397-7_1 (2006).
636 7 Zanini, F. *et al.* Population genomics of intrapatient HIV-1 evolution. *Elife* **4**, e11282,
637 doi:10.7554/eLife.11282 (2015).
638 8 Lythgoe, K. A. & Fraser, C. New insights into the evolutionary rate of HIV-1 at the within-host
639 and epidemiological levels. *Proceedings of the Royal Society B-Biological Sciences* **279**, 3367-3375,
640 doi:10.1098/rspb.2012.0595 (2012).
641 9 Hedskog, C. *et al.* Dynamics of HIV-1 Quasispecies during Antiviral Treatment Dissected
642 Using Ultra-Deep Pyrosequencing. *PloS one* **5**, e11345, doi:ARTN e11345
643 10.1371/journal.pone.0011345 (2010).
644 10 Shankarappa, R. *et al.* Consistent viral evolutionary changes associated with the progression
645 of human immunodeficiency virus type 1 infection. *J Virol* **73**, 10489-10502,
646 doi:10.1128/JVI.73.12.10489-10502.1999 (1999).
647 11 Masikini, P. & Mpondo, B. C. HIV drug resistance mutations following poor adherence in HIV-
648 infected patient: a case report. *Clin Case Rep* **3**, 353-356, doi:10.1002/ccr3.254 (2015).
649 12 TenoRes Study, G. Global epidemiology of drug resistance after failure of WHO
650 recommended first-line regimens for adult HIV-1 infection: a multicentre retrospective cohort study.
651 *Lancet Infect Dis* **16**, 565-575, doi:10.1016/S1473-3099(15)00536-8 (2016).
652 13 Collier, D. *et al.* Virological Outcomes of Second-line Protease Inhibitor-Based Treatment for
653 Human Immunodeficiency Virus Type 1 in a High-Prevalence Rural South African Setting: A
654 Competing-Risks Prospective Cohort Analysis. *Clinical infectious diseases : an official publication of*
655 *the Infectious Diseases Society of America* **64**, 1006-1016, doi:10.1093/cid/cix015 (2017).
656 14 Giandhari, J. *et al.* Genetic Changes in HIV-1 Gag-Protease Associated with Protease
657 Inhibitor-Based Therapy Failure in Pediatric Patients. *AIDS Res Hum Retroviruses* **31**, 776-782,
658 doi:10.1089/AID.2014.0349 (2015).

659 15 Kelly Pillay, S., Singh, U., Singh, A., Gordon, M. & Ndungu, T. Gag drug resistance mutations
660 in HIV-1 subtype C patients, failing a protease inhibitor inclusive treatment regimen, with detectable
661 lopinavir levels. *Journal of the International AIDS Society* **17**, 19784 (2014).
662 16 Sutherland, K. A. *et al.* Evidence for Reduced Drug Susceptibility without Emergence of
663 Major Protease Mutations following Protease Inhibitor Monotherapy Failure in the SARA Trial. *PloS*
664 *one* **10**, e0137834, doi:10.1371/journal.pone.0137834 (2015).
665 17 Sutherland, K. A. *et al.* Phenotypic characterization of virological failure following
666 lopinavir/ritonavir monotherapy using full-length Gag-protease genes. *The Journal of antimicrobial*
667 *chemotherapy* **69**, 3340-3348, doi:10.1093/jac/dku296 (2014).
668 18 Sutherland, K. A. *et al.* Gag-Protease Sequence Evolution Following Protease Inhibitor
669 Monotherapy Treatment Failure in HIV-1 Viruses Circulating in East Africa. *AIDS research and human*
670 *retroviruses* **31**, 1032-1037, doi:10.1089/aid.2015.0138 (2015).
671 19 Day, C. L. *et al.* Proliferative capacity of epitope-specific CD8 T-cell responses is inversely
672 related to viral load in chronic human immunodeficiency virus type 1 infection. *Journal of virology*
673 **81**, 434-438, doi:10.1128/JVI.01754-06 (2007).
674 20 Blanch-Lombarte, O. *et al.* HIV-1 Gag mutations alone are sufficient to reduce darunavir
675 susceptibility during virological failure to boosted PI therapy. *The Journal of antimicrobial*
676 *chemotherapy* **75**, 2535-2546, doi:10.1093/jac/dkaa228 (2020).
677 21 Feder, A. F. *et al.* More effective drugs lead to harder selective sweeps in the evolution of
678 drug resistance in HIV-1. *Elife* **5**, e10670, doi:10.7554/eLife.10670 (2016).
679 22 Harris, R. B., Sackman, A. & Jensen, J. D. On the unfounded enthusiasm for soft selective
680 sweeps II: Examining recent evidence from humans, flies, and viruses. *PLoS genetics* **14**, e1007859,
681 doi:10.1371/journal.pgen.1007859 (2018).
682 23 Dam, E. *et al.* Gag mutations strongly contribute to HIV-1 resistance to protease inhibitors in
683 highly drug-experienced patients besides compensating for fitness loss. *PLoS pathogens* **5**, e1000345
684 (2009).
685 24 Cong, M. E., Heneine, W. & Garcia-Lerma, J. G. The fitness cost of mutations associated with
686 human immunodeficiency virus type 1 drug resistance is modulated by mutational interactions.
687 *Journal of Virology* **81**, 3037-3041, doi:10.1128/Jvi.02712-06 (2007).
688 25 Wilke, C. O. Quasispecies theory in the context of population genetics. *BMC Evol Biol* **5**, 44,
689 doi:10.1186/1471-2148-5-44 (2005).
690 26 Lauring, A. S. & Andino, R. Quasispecies theory and the behavior of RNA viruses. *PLoS*
691 *Pathog* **6**, e1001005, doi:10.1371/journal.ppat.1001005 (2010).

27 Iwuji, C. C. *et al.* Evaluation of the impact of immediate versus WHO recommendations-guided antiretroviral therapy initiation on HIV incidence: the ANRS 12249 TasP (Treatment as Prevention) trial in Hlabisa sub-district, KwaZulu-Natal, South Africa: study protocol for a cluster randomised controlled trial. *Trials* **14**, 230, doi:10.1186/1745-6215-14-230 (2013).

28 World Health Organization. *Consolidated guidelines on the use of antiretroviral drugs for treating and preventing HIV infection: recommendations for a public health approach*. (World Health Organization, 2016).

29 Pang, J. *et al.* Haplotype assignment of longitudinal viral deep-sequencing data using co-variation of variant frequencies. *bioRxiv*, 444877, doi:10.1101/444877 (2020).

30 Cox, M. A. & Cox, T. F. in *Handbook of data visualization* 315-347 (Springer, 2008).

31 Stephens, M. & Scheet, P. Accounting for Decay of Linkage Disequilibrium in Haplotype Inference and Missing-Data Imputation. *The American Journal of Human Genetics* **76**, 449-462, doi:https://doi.org/10.1086/428594 (2005).

32 Song, H. *et al.* Tracking HIV-1 recombination to resolve its contribution to HIV-1 evolution in natural infection. *Nature Communications* **9**, 1928, doi:10.1038/s41467-018-04217-5 (2018).

33 Datir, R. *et al.* In Vivo Emergence of a Novel Protease Inhibitor Resistance Signature in HIV-1 Matrix. *mBio* **11**, e02036-02020, doi:10.1128/mBio.02036-20 (2020).

34 Kletenkov, K. *et al.* Role of Gag mutations in PI resistance in the Swiss HIV cohort study: bystanders or contributors? *J Antimicrob Chemother* **72**, 866-875, doi:10.1093/jac/dkw493 (2017).

35 Rabi, S. A. *et al.* Multi-step inhibition explains HIV-1 protease inhibitor pharmacodynamics and resistance. *The Journal of clinical investigation* **123**, 3848-3860, doi:10.1172/JCI67399 (2013).

36 Manasa, J. *et al.* Evolution of gag and gp41 in Patients Receiving Ritonavir-Boosted Protease Inhibitors. *Sci Rep* **7**, 11559, doi:10.1038/s41598-017-11893-8 (2017).

37 Datir, R., El Bouzidi, K., Dakum, P., Ndembi, N. & Gupta, R. K. Baseline PI susceptibility by HIV-1 Gag-protease phenotyping and subsequent virological suppression with PI-based second-line ART in Nigeria. *The Journal of antimicrobial chemotherapy* **74**, 1402-1407, doi:10.1093/jac/dkz005 (2019).

38 Parikh, U. M., Zelina, S., Sluis-Cremer, N. & Mellors, J. W. Molecular mechanisms of bidirectional antagonism between K65R and thymidine analog mutations in HIV-1 reverse transcriptase. *Aids* **21**, 1405-1414 (2007).

39 Parikh, U. M., Bacheler, L., Koontz, D. & Mellors, J. W. The K65R mutation in human immunodeficiency virus type 1 reverse transcriptase exhibits bidirectional phenotypic antagonism with thymidine analog mutations. *Journal of virology* **80**, 4971-4977 (2006).

725 40 Parikh, U. M., Barnas, D. C., Faruki, H. & Mellors, J. W. Antagonism between the HIV-1
726 reverse-transcriptase mutation K65R and thymidine-analogue mutations at the genomic level. *The*
727 *Journal of infectious diseases* **194**, 651-660 (2006).
728 41 Department of Health. 2019 ART Clinical Guidelines for the Management of HIV in Adults,
729 Pregnancy, Adolescents, Children, Infants and Neonates. (Republic of South Africa National
730 Department of Health, 2019).
731 42 UNAIDS. *Global HIV & AIDS statistics — 2020 fact sheet*,
732 <https://www.unaids.org/en/resources/fact-sheet> (2020), Accessed 3rd March 2021.
733 43 Gupta, R. K. *et al.* HIV-1 drug resistance before initiation or re-initiation of first-line
734 antiretroviral therapy in low-income and middle-income countries: a systematic review and meta-
735 regression analysis. *Lancet Infect Dis* **18**, 346-355, doi:10.1016/S1473-3099(17)30702-8 (2018).
736 44 Gupta, R. K. *et al.* Global trends in antiretroviral resistance in treatment-naive individuals
737 with HIV after rollout of antiretroviral treatment in resource-limited settings: a global collaborative
738 study and meta-regression analysis. *Lancet* **380**, 1250-1258, doi:10.1016/S0140-6736(12)61038-1
739 (2012).
740 45 Gregson, J. *et al.* Occult HIV-1 drug resistance to thymidine analogues following failure of
741 first-line tenofovir combined with a cytosine analogue and nevirapine or efavirenz in sub Saharan
742 Africa: a retrospective multi-centre cohort study. *Lancet Infect Dis*, doi:10.1016/S1473-
743 3099(16)30469-8 (2017).
744 46 WHO, C. Global Fund. HIV drug resistance report. 2017. *World Health Organisation* (2017).
745 47 Stefic, K., Bouvin-Pley, M., Braibant, M. & Barin, F. Impact of HIV-1 Diversity on Its Sensitivity
746 to Neutralization. *Vaccines (Basel)* **7**, 74, doi:10.3390/vaccines7030074 (2019).
747 48 Pancera, M. *et al.* Structure and immune recognition of trimeric pre-fusion HIV-1 Env.
748 *Nature* **514**, 455-461, doi:10.1038/nature13808 (2014).
749 49 Yu, F. *et al.* The Transmission and Evolution of HIV-1 Quasispecies within One Couple: a
750 Follow-up Study based on Next-Generation Sequencing. *Scientific reports* **8**, 1404,
751 doi:10.1038/s41598-018-19783-3 (2018).
752 50 Pang, J. *et al.* Mixed cytomegalovirus genotypes in HIV-positive mothers show
753 compartmentalization and distinct patterns of transmission to infants. *Elife* **9**, e63199,
754 doi:10.7554/eLife.63199 (2020).
755 51 Boshier, F. A. T. *et al.* Remdesivir induced viral RNA and subgenomic RNA suppression, and
756 evolution of viral variants in SARS-CoV-2 infected patients. *medRxiv*, 2020.2011.2018.20230599,
757 doi:10.1101/2020.11.18.20230599 (2020).

52 Parry, C. M. *et al.* Three residues in HIV-1 matrix contribute to protease inhibitor susceptibility and replication capacity. *Antimicrobial agents and chemotherapy* **55**, 1106-1113, doi:10.1128/AAC.01228-10 (2011).

53 Neher, R. A. & Leitner, T. Recombination rate and selection strength in HIV intra-patient evolution. *PLoS Comput Biol* **6**, e1000660, doi:10.1371/journal.pcbi.1000660 (2010).

54 El Bouzidi, K. *et al.* High prevalence of integrase mutation L74I in West African HIV-1 subtypes prior to integrase inhibitor treatment. *J Antimicrob Chemother* **75**, 1575-1579, doi:10.1093/jac/dkaa033 (2020).

55 Derache, A. *et al.* Predicted antiviral activity of tenofovir versus abacavir in combination with a cytosine analogue and the integrase inhibitor dolutegravir in HIV-1-infected South African patients initiating or failing first-line ART. *The Journal of antimicrobial chemotherapy*, doi:10.1093/jac/dky428 (2018).

56 Siedner, M. J. *et al.* Reduced efficacy of HIV-1 integrase inhibitors in patients with drug resistance mutations in reverse transcriptase. *Nat Commun* **11**, 5922, doi:10.1038/s41467-020-19801-x (2020).

57 Iwuji, C. *et al.* Universal test and treat is not associated with sub-optimal antiretroviral therapy adherence in rural South Africa: the ANRS 12249 TasP trial. *J Int AIDS Soc* **21**, e25112, doi:10.1002/jia2.25112 (2018).

58 Derache, A. *et al.* Impact of Next-generation Sequencing Defined Human Immunodeficiency Virus Pretreatment Drug Resistance on Virological Outcomes in the ANRS 12249 Treatment-as-Prevention Trial. *Clinical infectious diseases : an official publication of the Infectious Diseases Society of America* **69**, 207-214, doi:10.1093/cid/ciy881 (2019).

59 Gall, A. *et al.* Universal amplification, next-generation sequencing, and assembly of HIV-1 genomes. *Journal of clinical microbiology* **50**, 3838-3844, doi:10.1128/JCM.01516-12 (2012).

60 Martin, M. J. E. j. Cutadapt removes adapter sequences from high-throughput sequencing reads. **17**, pp. 10-12 (2011).

61 Li, H. Minimap2: pairwise alignment for nucleotide sequences. *Bioinformatics (Oxford, England)* **34**, 3094-3100, doi:10.1093/bioinformatics/bty191 (2018).

62 Shafer, R. W. Rationale and uses of a public HIV drug-resistance database. *The Journal of infectious diseases* **194 Suppl 1**, S51-58, doi:10.1086/505356 (2006).

63 Okonechnikov, K., Conesa, A. & Garcia-Alcalde, F. Qualimap 2: advanced multi-sample quality control for high-throughput sequencing data. *Bioinformatics (Oxford, England)* **32**, 292-294, doi:10.1093/bioinformatics/btv566 (2016).

64 Koboldt, D. C. *et al.* VarScan 2: somatic mutation and copy number alteration discovery in cancer by exome sequencing. *Genome Res* **22**, 568-576, doi:10.1101/gr.129684.111 (2012).

65 Charles, O. J., Venturini, C. & Breuer, J. cmvdrg - An R package for Human Cytomegalovirus antiviral Drug Resistance Genotyping. *bioRxiv*, 2020.2005.2015.097907, doi:10.1101/2020.05.15.097907 (2020).

66 Perrier, M. *et al.* Evaluation of different analysis pipelines for the detection of HIV-1 minority resistant variants. *PloS one* **13**, e0198334, doi:10.1371/journal.pone.0198334 (2018).

67 Minh, B. Q. *et al.* IQ-TREE 2: New models and efficient methods for phylogenetic inference in the genomic era. *bioRxiv*, 849372, doi:10.1101/849372 (2019).

68 Minh, B. Q., Nguyen, M. A. & von Haeseler, A. Ultrafast approximation for phylogenetic bootstrap. *Mol Biol Evol* **30**, 1188-1195, doi:10.1093/molbev/mst024 (2013).

69 Charles, O. J., Roberts, J., Breuer, J. & Goldstein, R. A. WeightedLD: The Application of Sequence Weights to Linkage Disequilibrium. *bioRxiv*, 2021.2006.2004.447093, doi:10.1101/2021.06.04.447093 (2021).

70 Martin, D. P. *et al.* RDP5: a computer program for analyzing recombination in, and removing signals of recombination from, nucleotide sequence datasets. *Virus Evol* **7**, veaa087, doi:10.1093/ve/veaa087 (2021).

Table 1. Regimens and viral load at final timepoint for all participants. Participants initiated and maintained 1st-line regimens for between 1-10 years before being switched to 2nd-line regimens as part of the TasP trial. Eight of the nine participants were failing 2nd-line regimens at the final timepoint.

Participant	No. of timepoints	1st-line regimen	Time since initiation of 1st-line treatment (yrs.)	2nd-line regimen	Viral Load at final timepoint (copies/ml)
15664	6	d4T, 3TC, FTC	6.2	LPV/r, TDF, FTC	28655
16207	5	d4T, 3TC, NVP	5.9	LPV/r, TDF, FTC	56660
22763	8	d4T, 3TC, EFV	6.2	LPV/r, TDF, 3TC	15017
22828	6	d4T, 3TC, NVP	6.4	LPV/r, TDF, 3TC/FTC	947
26892	7	d4T, 3TC, EFV	6	LPV/r, TDF, FTC	12221
28545	5	TDF, FTC, EFV	1.3	LPV/r, AZT, 3TC	12964
29447	4	TDF, FTC, EFV	2.8	LPV/r, TDF, FTC	64362
47939	3	d4T, 3TC, EFV	10.1	LPV/r, AZT, 3TC/FTC	6328

NRTI: Stavudine, d4T; Lamivudine, 3TC; Tenofovir, TDF; Emtricitabine, FTC; Zidovudine, AZT. **NNRTI:** Efavirenz, EFV; Nevirapine, NVP. **PI:** Lopinavir/ritonavir, LPV/r.

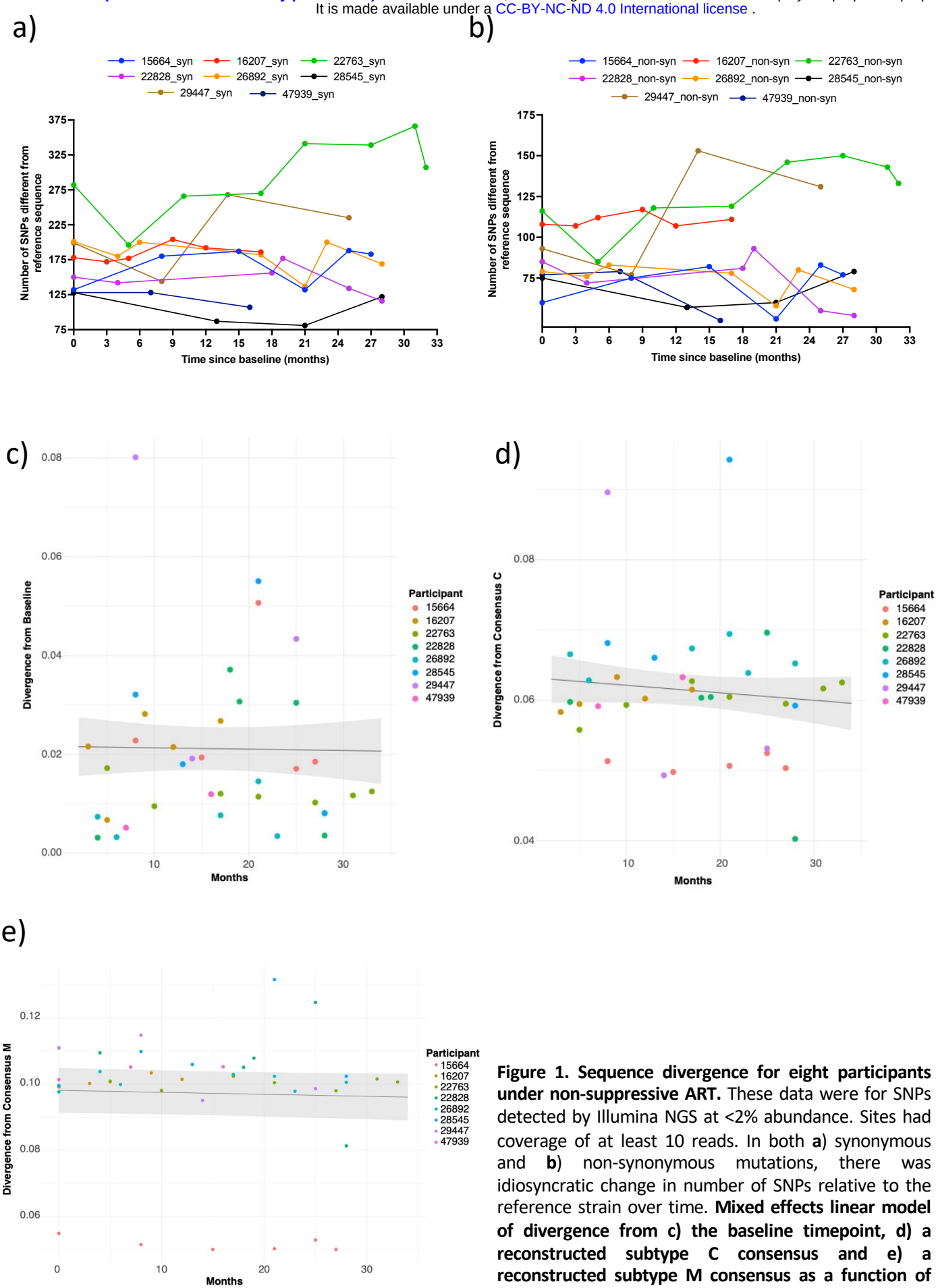

Figure 1. Sequence divergence for eight participants under non-suppressive ART. These data were for SNPs detected by Illumina NGS at <2% abundance. Sites had coverage of at least 10 reads. In both **a**) synonymous and **b**) non-synonymous mutations, there was idiosyncratic change in number of SNPs relative to the reference strain over time. **Mixed effects linear model of divergence from c) the baseline timepoint, d) a reconstructed subtype C consensus and e) a reconstructed subtype M consensus as a function of time (months).**

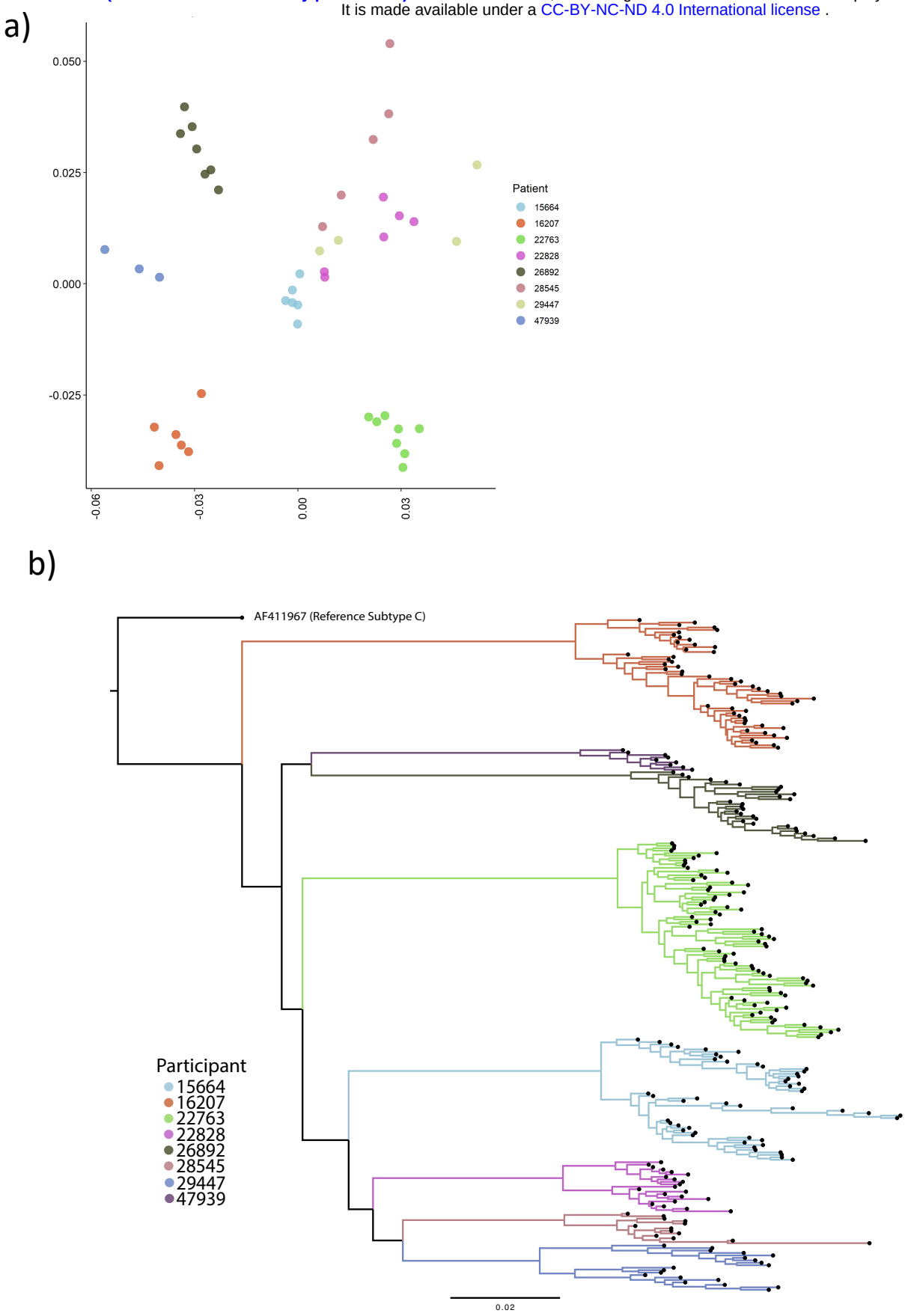

Figure 2. Multi-dimensional scaling showing A) clustering of HIV whole genomes from consensus sequences with high intra-participant diversity. Multi-dimensional scaling (MDS) were created by determining all pairwise distance comparisons under a TN93 substitution model, coloured by participant. Axis are MDS-1 and MDS-2. **B) Maximum likelihood phylogeny of constructed viral haplotypes for all participants**. The phylogeny was rooted on the AF411967 clade C reference genome. Reconstructed haplotypes were genetically diverse and did not typically cluster by timepoint.

A)

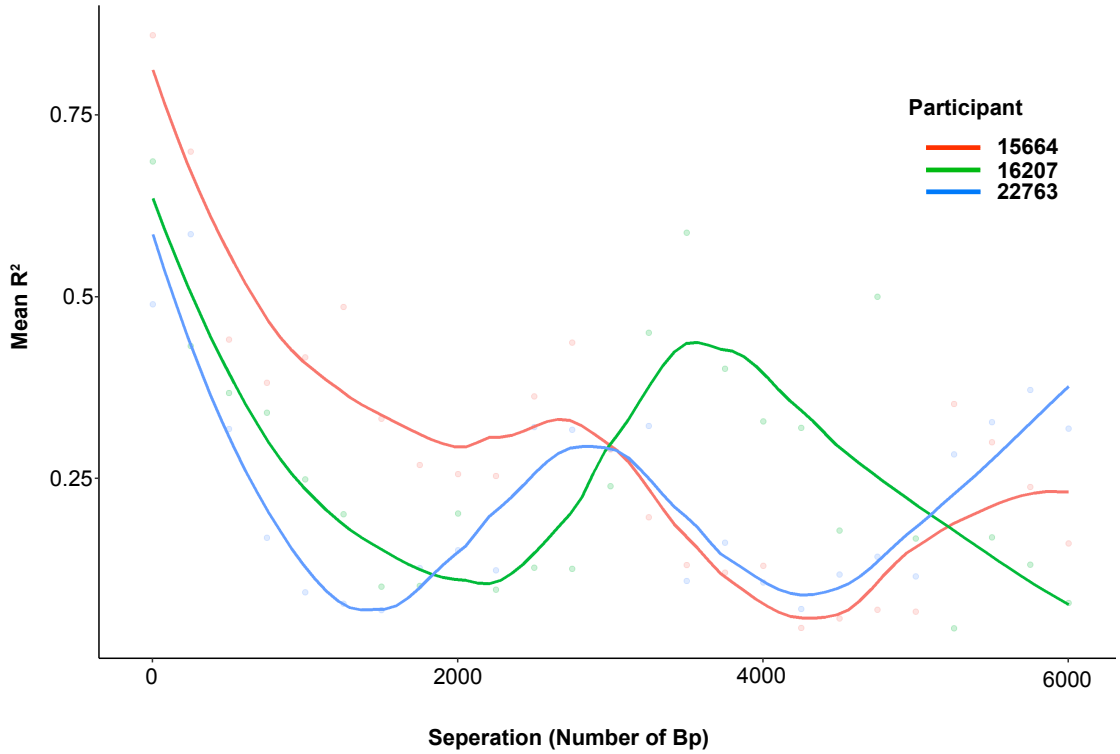

B)

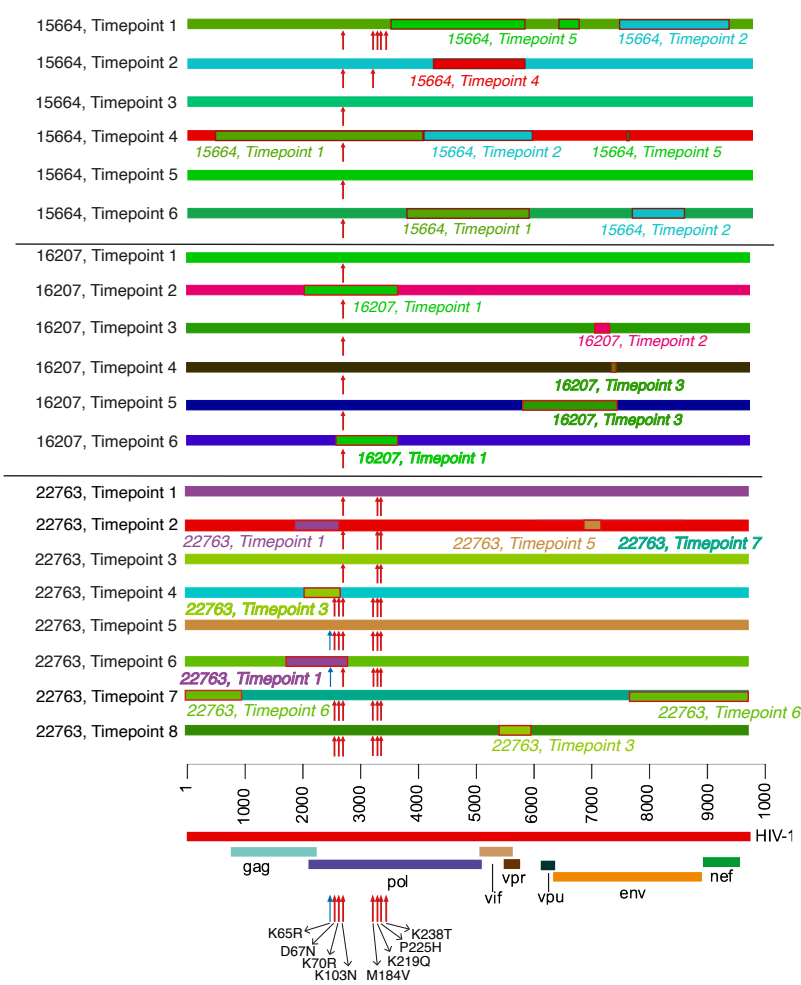

Figure 3A) Pairwise linkage disequilibrium decays rapidly with increasing distance between SNPs. The line indicates the average LD of all eight patients. There was a constant decrease in linkage disequilibrium over the first 800bp. **B) Putative recombination breakpoints and drug-resistance associated mutations of all longitudinal consensus sequences belonging to three participants: 15664, 16207 and 22763**. All sequences were coloured uniquely uniquely; perceived recombination events supported by 4 or more methods implemented in RDP5 are highlighted with a red border and italic text to show the major parent and recombinant portion of the sequence. Drug-resistance associated mutations are indicated with a red arrow, relative to the key at the bottom of the image. For ease of distinguishment, the K65R mutations is indicated with a blue arrow.

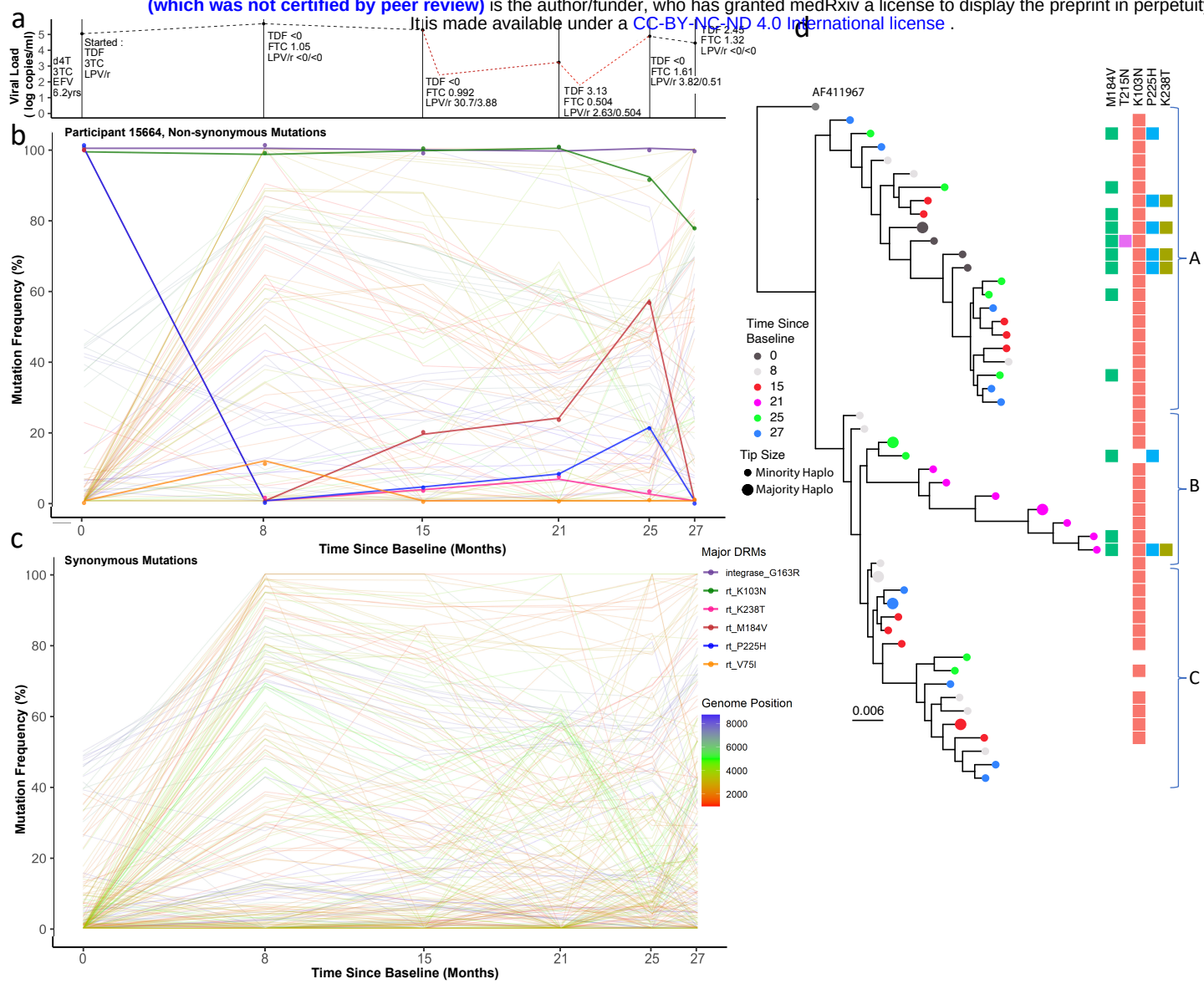

Figure 4. Drug regimen, adherence and viral dynamics within participant 15664. a) Viral load and drug levels. At successive timepoints drug regimen was noted and plasma drug concentration measured by HPLC (nmol/l). The participant was characterised by multiple partial suppression (<750 copies/ml, 16 months; <250 copies/ml, 22 months) and rebound events (red dotted line) and poor adherence to the drug regimen. **b) Drug resistance and non-drug resistance associated non-synonymous mutation frequencies by Illumina NGS.** The participant had large population shifts between timepoints 1-2, consistent with a hard selective sweep, coincident with the shift from 1st-line regimen to 2nd-line. **c) Synonymous mutation frequencies.** All mutations with a frequency of <10% or >90% at two or more timepoints were tracked over successive timepoints. Most changes were restricted to *gag* and *pol* regions and had limited shifts in frequency i.e. between 20-60%. **d) Maximum-likelihood phylogeny of reconstructed haplotypes.** Haplotypes largely segregated into three major clades (labelled A-C). Majority and minority haplotypes, some carrying lamivudine resistance mutation M184V. Clades referred to in the text body are shown to the right of the heatmap.

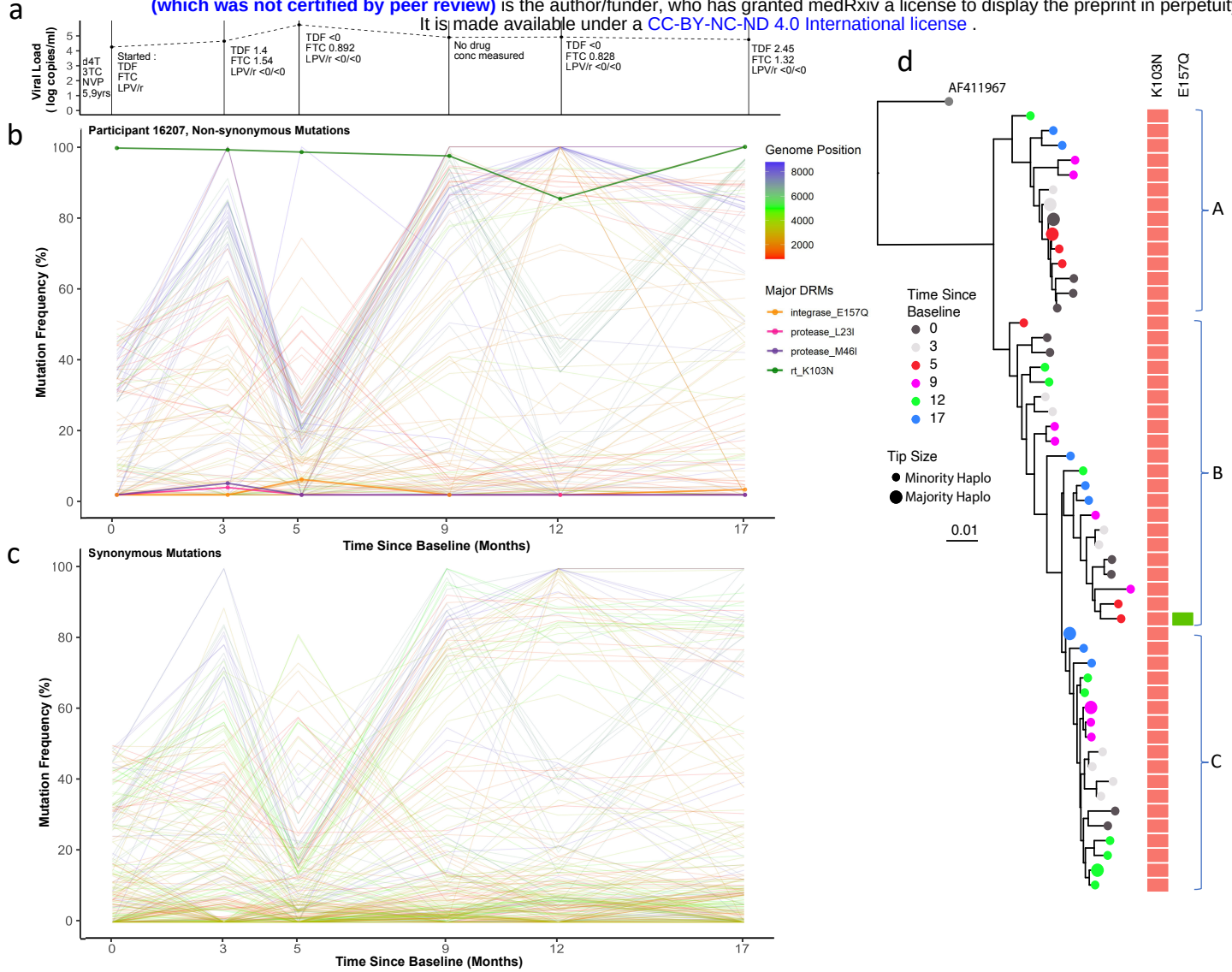

Figure 5. Drug regimen, adherence and viral dynamics within participant 16207. A) Viral load and drug levels. At successive timepoints regimen was noted and plasma drug concentration measured by HPLC (nmol/l). The participant displayed ongoing viraemia and poor adherence to the prescribed drug regimen. **B) Drug resistance and non-drug resistance associated non-synonymous mutations frequencies.** The participant had only one major RT mutation - K103N for the duration of the treatment period. Several antagonistic non-synonymous switches in predominantly *env* were observed between timepoints 1-4. **C) Synonymous mutation frequencies.** All mutations with a frequency of <10% or >90% at two or more timepoints were followed over successive timepoints. In contrast to non-synonymous mutations, most synonymous changes were in *pol*, indicative of linkage to the env coding changes. **D) Maximum-likelihood phylogeny of reconstructed haplotypes.** Haplotypes were again clearly divided intro three distinct clades; each clade contained haplotypes from all timepoints, suggesting lack of hard selective sweeps and intermingling of viral haplotypes with softer sweeps. that most viral competition occurred outside of drug pressure.

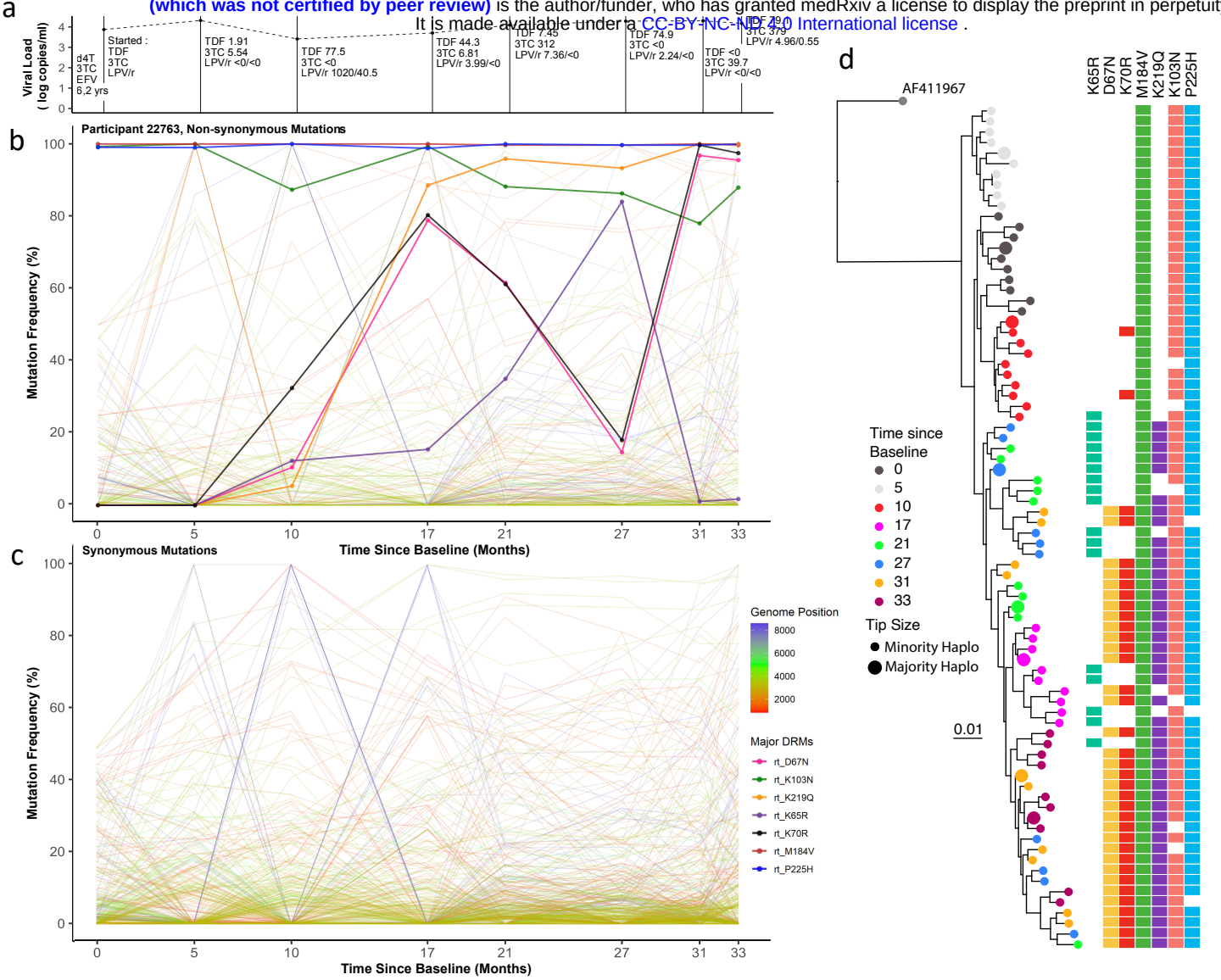

Figure 6. Drug regimen, adherence and viral dynamics of participant 22763. A) Viral load and regimen adherence. At successive timepoints the regimen was noted, and plasma drug concentration measured by HPLC (nmol/l). The participant had therapeutic levels of drug at several timepoints (3, 5 and 8), indicating variable adherence to the prescribed drug regimen. **B) Drug resistance and non-drug-resistance-associated non-synonymous mutation frequencies.** The participant had numerous drug resistance mutations in dynamic flux. Between timepoints 4-7, there was a complete population shift, indicated by reciprocal competition between the RT mutations K65R and the TAMs K67N and K70R. **C) Synonymous mutations frequencies.** All mutations with a frequency of <10% or >90% at two or more timepoints were followed over successive timepoints. Several *env mutations* mimicked the non-synonymous shifts observed between timepoints 2-4, suggestive of linkage. **D) Maximum-likelihood phylogeny of reconstructed haplotypes.** timepoints 1-4 were found in distinct lineages. In later timepoints, from 5-8, haplotypes became more intermingled, whilst maintaining antagonism between K65R and K67N bearing viruses.